

# Molecularly Adsorbed Oxygen Species on Si(111)-(7×7): STM-Induced Dissociative Attachment Studies

R. Martel, Ph. Avouris,\* I.-W. Lyo

Scanning tunneling microscope (STM)-induced selective bond breaking in individual molecules and conventional STM imaging are combined to determine the nature of chemisorbed O<sub>2</sub> species formed during the initial stages of silicon (111)-(7×7) oxidation. A selective atomic-scale modification mechanism that involves dissociative electron attachment of tip-emitted electrons to empty adsorbate orbitals is introduced. Two molecular species were found: one involves O<sub>2</sub> bonded to an already oxidized silicon adatom, and the other involves an O<sub>2</sub> molecule that is bonded to a second-layer rest atom and interacting with two silicon adatoms.

The STM has been used successfully to obtain information on surface chemistry at the atomic scale (1). However, unambiguous identification of the structure of the reaction products is not always possible. The lack of chemical selectivity has been a serious impediment in chemical applications of the STM. On the other hand, the STM can also be a powerful atomic-scale modification tool (2). Strong electric fields (3) and the excitations induced by the STM (4) can break strong chemical bonds. Here we combine the imaging and bond-breaking capabilities of the STM to identify the chemisorbed O<sub>2</sub> species, usually referred to as molecular precursors, formed during the initial stages of the oxidation of the Si(111)-(7×7) surface. We selectively break the O-O bond by resonant capture of tip-emitted electrons in empty O<sub>2</sub> energy levels in order to isolate the oxidation products.

Numerous experimental and theoretical studies have been made of the initial oxidation of Si(111) (5). For example, x-ray photoemission spectroscopy (XPS) has shown that early on in the reaction, Si atoms in a variety of oxidation states are present (6), which indicates that several different products are formed. Vibrational spectroscopy detects strong Si-O-Si vibrations, showing that a major reaction channel involves insertion of O atoms in Si-Si bonds (6-8). The stability of such a structure is confirmed by electronic structure calculations (9-11). In addition to the stable atomic-oxygen products, a molecularly chemisorbed O<sub>2</sub> species was detected in the initial stages of oxidation through its vibrational (7, 8, 12) and photoelectron spectra (13-15). It has generally been assumed that this molecular species is the precursor to stable oxidation products involving atomic oxygen. Its lifetime was initially reported to be ~10 min at room

temperature (13). More recently, the lifetime was found to be much longer: one source says ~1 hour (16), whereas another study reports 5 hours (17). Furthermore, spectroscopic investigations (18) provide evidence for two, not one, types of long-lived molecular species. However, it was also found that products containing atomic oxygen are present immediately after exposure to O<sub>2</sub>, even at cryogenic temperatures, at which the precursor should be stable (7, 12, 19). These contradictory observations led us to investigate the Si(111)-(7×7) oxidation with STM-based atomic-scale modification techniques. The experimental system and sample preparation procedures have been described elsewhere (20).

The schematic representation of the 7×7 structure in Fig. 1 depicts only the sites bearing dangling bonds (that is, the top-layer Si atoms, the so-called adatoms) (large open circles), the second-layer rest atoms (medium filled circles), and corner-hole atoms (small filled circles). These are the most likely sites of initial reactivity (5).

In Fig. 2, we show two STM images of the same area of a Si(111)-(7×7) surface exposed at room temperature to differing amounts of O<sub>2</sub>. They show the unreacted top-layer Si atoms (adatoms, labeled N) and a number of product sites induced by O<sub>2</sub> exposure. We will refer to the products as "bright" (B) or "dark" (D), depending on whether they appear brighter or darker than unreacted Si adatoms in constant-current STM images. The B products involve single adatom sites and are the most numerous product at low exposures. The D products could be formed at single adatom sites or may involve two adjacent adatom sites (labeled as D and DD, respectively); they dominate the STM images for exposures >0.6 L (1 L = 10<sup>-6</sup> torrs).

Contrast variations in an STM image depend on the density of states  $\rho_s^i(E)$  at a particular site  $i$  and energy  $E$  and on the rate of this density's decay ( $\kappa$ ) in the  $z$

direction (height above the surface), which in turn depends on the height of the local tunneling barrier (21). A chemical reaction at site  $i$  can change not only  $\rho_s^i(E)$  but also  $\kappa$  by generating dipoles that add to or subtract from the inward-pointing surface dipole, thus increasing or decreasing, respectively, the surface work function (22). The latter effect is particularly important when elements of very different electronegativity, such as Si and O, are involved. Calculations of  $\rho_s^i(E)$  for a variety of surface structures containing atomic oxygen and consideration of the effects of the resulting dipoles on the barrier height show that an O atom inserted into surface Si back bonds generates a product that appears bright in the STM image, whereas oxygen bonded on top of Si leads to a dark site (11, 14, 23).

Although the Si(111) surface should contain significant amounts (>20%) of chemisorbed O<sub>2</sub> at room temperature (13), the STM images (Fig. 2) do not provide direct evidence of chemisorbed oxygen. The images are stable; that is, they do not reveal significant changes in the numbers and distributions of bright and dark sites as a function of time under good, ultrahigh-vacuum conditions. To locate the chemisorbed O<sub>2</sub> species, we used the STM to locally induce their desorption or dissociation by means of a process specific to the O-O bond. This bond-breaking mechanism involves the transient occupation of empty levels; here, we used the  $3\sigma_u^*$  "shape resonance" (24) of chemisorbed O<sub>2</sub>, by tip-emitted elec-

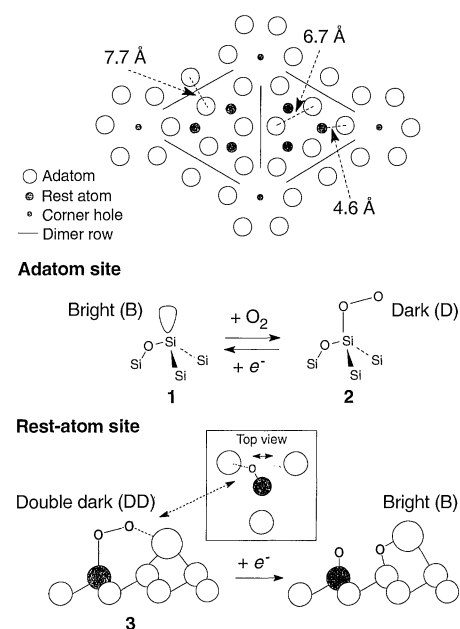


**Fig. 1.** (Top) Schematic representation of the structure of the Si(111)-(7×7) surface showing the unit cell and the sites bearing dangling bonds. (Bottom) Reactions producing the molecular chemisorbed O<sub>2</sub> (species **2** and **3**) and their electron-induced destruction channels; **1** is on an atomic-oxygen site.

trons, a process that can be described as dissociative electron attachment (25). In the free  $O_2$  molecule, the  $3\sigma_u^*$  level is strongly antibonding and lies  $\sim 9$  eV above the vacuum level (24). Chemisorption of  $O_2$  transfers charges from the substrate to the  $2\pi^*$  level of the molecule and significantly weakens and elongates the O-O bond, which reduces the  $3\sigma_u^*$  energy. For  $O_2$  chemisorbed on Pt(111) or Pd(111), the  $3\sigma_u^*$  is  $\sim 6$  eV above the Fermi energy  $E_F$  (26). Population of this state leads to  $O_2$  dissociation or desorption (26). Tight-binding calculations of the interaction of  $O_2$  with Si(111) (27) place the  $3\sigma_u^*$  level  $\sim 7$  eV above  $E_F$  for an O-O length of 1.28 Å, determined by near-edge x-ray fine structure spectroscopy (13). Experimentally, photofragmentation of the adsorbed  $O_2$  (15, 16) also places the  $3\sigma_u^*$  level in this energy range.

When an incident electron has the same energy as the  $3\sigma_u^*$  level of  $O_2$ , it can be captured to form a "resonance." Capture occurs because the centrifugal, Coulomb, polarization, and exchange forces acting on the electron combine to create a potential with a penetrable barrier surrounding the molecule (Fig. 3A) (24). Excitation arises from the following sequence of events (Fig. 3, B and C): (step 1) electron capture, (step 2) nuclear motion (relaxation) in the negative ion state, and (step 3) electron emission and formation of a vibrationally excited state. If the excitation exceeds the dissociation energy, fragmentation occurs (step 4) (24). In electronic excitation, all incident electron energies above the excitation threshold can induce excitation, whereas in the dissociative attachment process, only electrons within a relatively narrow energy range can be trapped. The change in the charge state of the adsorbate upon capture of an electron affects the charged adsorbate's interaction with its image in the substrate (28) and can open a new reaction channel (Fig. 3C). Because of the increased imagelike attraction to the substrate, the equilibrium adsorbate-substrate distance is smaller in this more strongly charged state than in the initial state, and

therefore, upon electron capture, the molecule moves toward the surface. Soon after, the trapped electron escapes, and the system undergoes an essentially vertical transition (no change in the position of the nuclei) to the repulsive part of the ground-state potential energy surface (Fig. 3C). If sufficient energy has been gained, the molecule can break the substrate-adsorbate bond and desorb (29). The decay mode of chemisorbed  $O_2$  (molecular dissociation or desorption) depends on its local bonding configuration.

The experiment involved several steps. First, the clean surface was imaged, exposed to small amounts of  $O_2$ , and imaged again to locate the primary product sites. The surface was then exposed to additional  $O_2$ , and the relation of the new reacted sites to the old ones was established. All imaging was performed at low bias ( $|V| \leq 2$  V) to avoid any decomposition processes induced by energetic electrons. Finally, the sample bias was increased in steps up to +15 V, the reacted area of the surface was scanned at each step, the voltage was lowered again, and the results of the scanning at high voltage (the irradiation by the high-energy electrons) were imaged. In this way, we detected changes induced by the STM at the different oxidation-produced sites.

The bright products occupy surface sites where the density of states near  $E_F$  is highest, thus making the sticking coefficient of  $O_2$  maximal for these pristine Si sites (14). Therefore, there is a good possibility that the B products are the molecular  $O_2$  (30). We found these sites to be stable at room temperature under good, ultrahigh vacuum. Furthermore, the sites survived heating up to 600 K. However, all published studies involving photoemission (13, 15), vibrational spectroscopy (7, 8), and second-harmonic generation (17) show the molecular species disappearing at  $\sim 450$  K. Second, electron irradiation did not produce any changes in the bright sites. Similarly, D sites present on the surface after  $O_2$  dosing and annealing (to dissociate  $O_2$ ) were not

affected by electron irradiation. Finally, we correlated STM images with XPS determination (11, 13) of the relative concentration of atomic and molecular species under the same conditions. For example, a 2.5-L  $O_2$  exposure shows a dark to bright ratio of 4:1, whereas the ratio of the coverage present in the molecular form is  $\sim 2:3$  (11, 13, 17). It is clear that there are not enough B sites to account for the molecular concentration determined by XPS. From the above evidence, we have to conclude that the B sites contain atomic oxygen and that a fraction of the D sites must contain molecular species. Molecular  $O_2$  sites may appear darker than the surrounding Si atoms in the STM images for two reasons: (i) the density of states near  $E_F$  of peroxy-type molecular species is predicted to be very low (27, 31) and (ii) the chemisorbed  $O_2$  is negatively charged by charge transfer [from the  $O_2$  vibrational frequency, an  $\sim 1e$  charge has been estimated (8, 13)]. Thus, a strong dipole pointing inward from the surface is generated that should increase the local work function (tunneling barrier). Experimentally, the Si work function increases drastically upon  $O_2$  exposure (19). After  $O_2$  exposure at room temperature, two types of D sites are present on the Si(111) surface that are quite sensitive to electron irradiation at 6 to 9 eV relative to  $E_F$ . This energy

**Fig. 2.** Empty-state STM images of a Si(111)-(7 $\times$ 7) surface (140 Å by 215 Å) during the early stages of oxidation ( $V_{\text{sample}} = 2$  V): (A) after exposure to 0.05 L of  $O_2$ , and (B) the same area after exposure to an additional 0.05 L of  $O_2$ . The arrows point to typical  $O_2$  reaction sites.

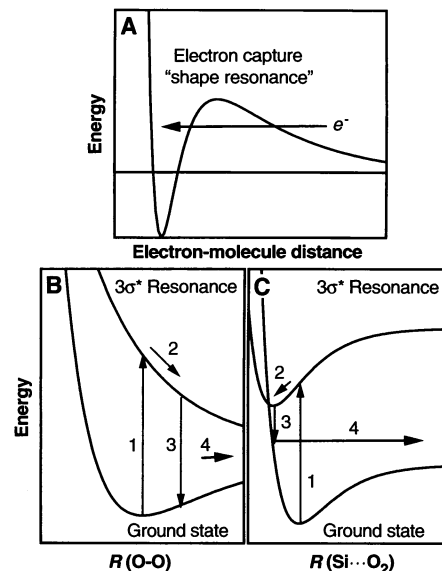
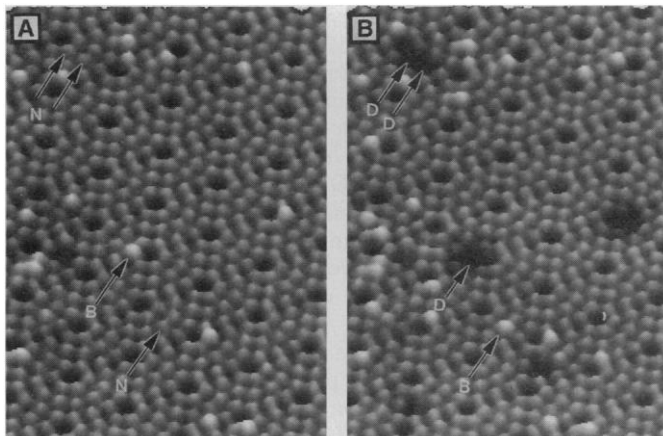


**Fig. 3.** (A) Schematic illustration of the potential that traps an incident electron in a "shape resonance." (B and C) Qualitative potential energy diagrams illustrating the sequence of events that lead to (B) molecular fragmentation and (C) desorption: (step 1) electron attachment, (step 2) nuclear motion (relaxation) in the negative ion force field, and (step 3) electron detrapping. In (B), step 4 leads to fragmentation either directly from the ionic potential energy surface or from the "hot" ground state, whereas in (C), step 4 leads to desorption from the "hot" ground-state surface.

is in agreement with other experimental (15, 16) and theoretical determinations (27) of the  $3\sigma^*$  energy. Infrequent spontaneous atomic rearrangements involving the same dark sites were also observed.

After exposure to 0.05 L of  $O_2$ , the dominant reaction products are B sites (arrow, Fig. 4A). Exposure to an additional 0.03 L of  $O_2$  (Fig. 4B) turns some B sites into D sites (32). By following the surface reaction as a function of  $O_2$  exposure, we determine the cross section for the formation of the D site from the B site (structure 1, Fig. 1) to be  $\sim 73 \text{ \AA}^2$ , which is at least 13 times the cross section for B site formation. An analogous behavior involving the reaction of the so-called C defects has been observed in the oxidation of the Si(100) surface (33).

Although these D sites appear to be stable at room temperature, they are unstable under electron irradiation. For sample

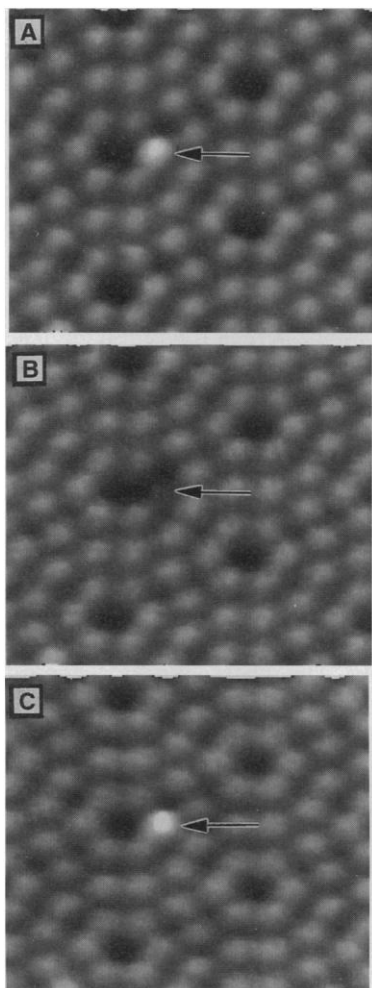


**Fig. 4.** Empty-state STM images of a Si(111)-(7 $\times$ 7) surface recorded (A) after exposure to 0.05 L of  $O_2$ , (B) after an additional exposure to 0.03 L of  $O_2$ , and (C) after a scan at sample bias  $V_{\text{sample}} = +7 \text{ V}$  and current  $I = 0.4 \text{ nA}$ . The arrows mark the  $O_2$ -induced B to D and electron-induced D to B product transformations.

biases near +7 V, they decompose by way of two channels. One important reaction channel regenerates the original B site (Fig. 4C), which suggests that the oxygen is not dissociated at these sites but is adsorbed molecularly on top of the bright site (structure 2, Fig. 1). By varying the time interval between the  $O_2$  exposure leading to the formation of the above molecular D sites and the irradiation scan, we can deduce that the lifetime of these sites is  $>3$  hours, in agreement with the lifetime deduced by Dujardin *et al.* (16). Along with the molecular desorption channel, we observe another

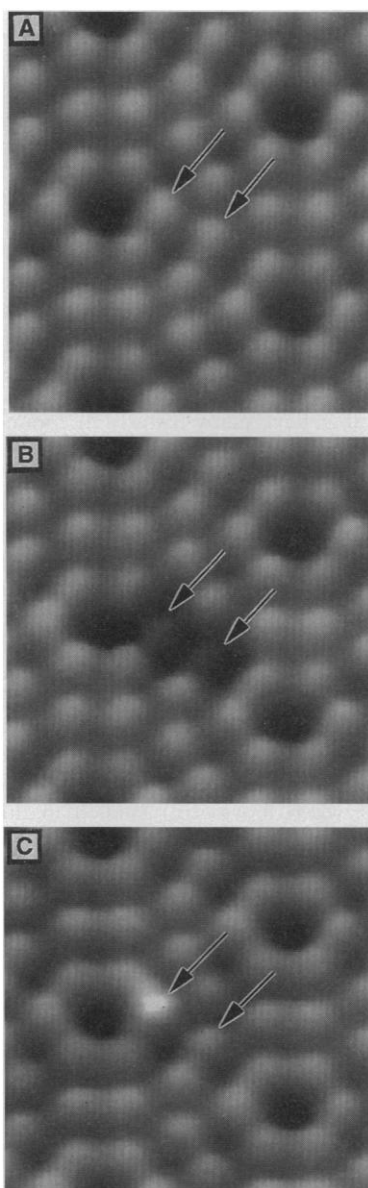


**Fig. 5.** Empty-state STM images of a Si(111)-(7 $\times$ 7) surface recorded (A) after exposure to 0.05 L of  $O_2$ , (B) after an additional exposure to 0.01 L of  $O_2$ , and (C) after a scan at  $V_{\text{sample}} = +7 \text{ V}$  and  $I = 0.4 \text{ nA}$ . The arrows mark the  $O_2$ -induced DD site and its electron irradiation-induced destruction, which generates a B corner adatom site and a normal adatom site.

reaction channel for the D sites that may involve electron-induced fragmentation. This channel results in an adatom site that appears "gray," that is, darker than normal.

A second type of molecularly chemisorbed species, a primary product of the oxidation process, is the DD site: two adjacent, somewhat darker adatoms (Fig. 2). The dependence of the formation of such sites to  $O_2$  exposure shows that they are formed in one step from the reaction of the surface with a single  $O_2$  molecule. Comparison of the surface after exposure to 0.05 L of  $O_2$  (Fig. 5A) and after exposure to an additional 0.01 L of  $O_2$  (Fig. 5B) shows the generation of the DD site (the arrows point to the same two adatoms). Invariably, one of the two Si adatoms is a corner adatom. If we now irradiate this DD site with 6-eV electrons, it decomposes. The major decomposition pathway changes one of the two D adatoms into a normal (unreacted) adatom, while the other is transformed into a B site (Fig. 5C). In most cases, the B site is formed at a corner site, that is, it has the same selectivity as the direct B-site formation process. Less often we see the regeneration of two unreacted Si adatoms, presumably by  $O_2$  desorption. Like the D-site molecular species, the DD species are long-lived at room temperature.

The structure of the DD site is by no means obvious. Two adatoms turning dark in a reaction with a single  $O_2$  molecule suggests perhaps a configuration similar to a bridge between the  $O_2$  and two adjacent adatoms. However, the Si(111)-(7 $\times$ 7) surface does not allow such a configuration: the distance between two adjacent adatoms is too large ( $\sim 7 \text{ \AA}$ ) to be bridged by  $O_2$ . On the other hand, a top-layer adatom and a second-layer rest atom are  $\sim 4.5 \text{ \AA}$  apart and could be bridged by a stretched  $O_2$  molecule. This bridged configuration would, however, form only one D adatom site, and calculations by Schubert *et al.* (27) suggest that it should be short lived.

Structure 3 (Fig. 1) is consistent with both the STM image and the observed chemistry. The  $O_2$  molecule is bonded with one end to a second-layer rest atom, while the O-O axis, which should be nearly parallel to the surface (27, 31), is confined between two adatoms with which the molecule interacts. Adatoms have a small positive charge due to charge transfer to rest atoms (20, 34), and  $O_2$  is negatively charged. At room temperature, the O-O axis is trapped between two adatoms but can oscillate between them. As a result of their interaction with  $O_2$  and the strong increase in the local tunneling barrier induced by the large Si- $O_2$  dipole, these two Si adatoms appear somewhat darker in the STM image than do their neighbors. When an electron is attached to the  $3\sigma^*$  level of

this structure, it breaks the O-O bond, leaving one O attached to the rest atom, while the other is inserted into a back bond of one of the two adatoms [the lowest energy position of an O atom bonded to an adatom (10)], leaving the second adatom intact. Thermal decomposition of the DD site also gives the same products.

## REFERENCES AND NOTES

1. Ph. Avouris, *J. Phys. Chem.* **94**, 2246 (1990); J. Boland, *Adv. Phys.* **42**, 129 (1993).
2. Ph. Avouris, *Acc. Chem. Res.* **28**, 95 (1995).
3. I.-W. Lyo and Ph. Avouris, *Science* **253**, 173 (1991); A. Kobayashi, F. Grey, E. Snyder, M. Aono, *Phys. Rev. B* **49**, 8067 (1994).
4. R. S. Becker, G. S. Higashi, Y. J. Chabal, A. J. Becker, *Phys. Rev. Lett.* **65**, 1917 (1990); J. Wintterlin and Ph. Avouris, *J. Chem. Phys.* **100**, 687 (1994); T.-C. Shen *et al.*, *Science* **268**, 1590 (1995).
5. T. Engel, *Surf. Sci. Rep.* **18**, 91 (1993).
6. G. Hollinger and F. J. Himpsel, *Phys. Rev. B* **28**, 3651 (1983).
7. H. Ibach, H. D. Bruchmann, H. Wagner, *Appl. Phys. A* **29**, 113 (1982).
8. K. Edamoto, Y. Kubota, H. Kobayashi, M. Onchi, M. Nishijima, *J. Chem. Phys.* **83**, 428 (1985).
9. I. P. Batra, P. S. Bagus, K. Hermann, *Phys. Rev. Lett.* **52**, 384 (1984).
10. X. M. Zheng and P. L. Cao, *Surf. Sci.* **219**, L543 (1989).
11. B. Schubert, Ph. Avouris, R. Hoffmann, *J. Chem. Phys.* **98**, 7606 (1993).
12. A. J. Schell-Sorokin and J. E. Demuth, *Surf. Sci.* **157**, 273 (1985).
13. U. Höfer, P. Morgen, W. Wurth, E. Umbach, *Phys. Rev. B* **40**, 1130 (1989).
14. Ph. Avouris, I.-W. Lyo, F. Bozso, *J. Vac. Sci. Technol. B* **9**, 424 (1991).
15. F. Bozso and Ph. Avouris, *Phys. Rev. B* **44**, 9129 (1991).
16. G. Dujardin *et al.*, *Phys. Rev. Lett.* **73**, 1727 (1994).
17. P. Bratu, K. L. Kompa, U. Höfer, *Phys. Rev. B* **49**, 14070 (1994).
18. G. Comtet *et al.*, *Surf. Sci.* **331-333**, 370 (1994).
19. C. Silvestre and M. Shayegan, *Phys. Rev. B* **37**, 10432 (1988).
20. Ph. Avouris and R. Wolkow, *ibid.* **39**, 5071 (1989).
21. J. Tersoff and D. R. Hamann, *ibid.* **31**, 805 (1994).
22. A. Zangwill, *Physics at Surfaces* (Cambridge Univ. Press, Cambridge, 1988).
23. Y. Ono, M. Tabe, H. Kageshima, *Phys. Rev. B* **48**, 14291 (1993).
24. G. J. Schulz, *Rev. Mod. Phys.* **45**, 423 (1973).
25. L. Sanche, *Phys. Rev. B* **23**, 1597 (1990).
26. H. Kuhlbeck *et al.*, *Chem. Phys. Lett.* **238**, 93 (1995).
27. B. Schubert, Ph. Avouris, R. Hoffmann, *J. Chem. Phys.* **98**, 7593 (1993).
28. J. E. Demuth, D. Schmeisser, Ph. Avouris, *Phys. Rev. Lett.* **47**, 1166 (1981).
29. J. W. Gadzuk, L. J. Richter, S. A. Buntin, D. S. King, R. R. Cavanagh, *Surf. Sci.* **235**, 317 (1990); C. P. Salam, M. Persson, R. E. Palmer, *Phys. Rev. B* **49**, 10655 (1994).
30. Ph. Avouris and I.-W. Lyo, in *Scanning Probe Microscopy*, H. K. Wickramasinghe, Ed. (AIP Conference Proceedings 241, American Institute of Physics, New York, 1992).
31. W. A. Goddard III, A. Redondo, T. C. McGill, *Solid State Commun.* **18**, 981 (1976).
32. J. P. Pelz and R. H. Koch, *J. Vac. Sci. Technol. B* **9**, 775 (1991).
33. Ph. Avouris and D. Cahill, *Ultramicroscopy* **42**, 838 (1992).
34. J. E. Northrup, *Phys. Rev. Lett.* **57**, 154 (1986).
35. R.M. acknowledges the receipt of a Fonds pour la Formation de Chercheurs et l'Aide à la Recherche (FCAR) Québec postdoctoral fellowship.

31 August 1995; accepted 22 February 1996

# Spatiotemporal Chaos in Electroconvection

Michael Dennin, Guenter Ahlers,\* David S. Cannell

Spatiotemporal chaos (STC) near the onset of electroconvection in a nematic liquid crystal is reported. In samples with conductivities greater than  $1 \times 10^{-8}$  per ohm per meter, STC was found to evolve by means of a supercritical Hopf bifurcation from the uniform conduction state. Because this example of STC resulted from nonlinear interactions between only four modes, it provides a realistic opportunity to understand the observed phenomena in terms of a weakly nonlinear theory in the form of four coupled complex Ginzburg-Landau equations derived from the full equations of motion of the system. For smaller conductivities, the pattern immediately above onset consisted of localized pulses of convection that coexisted with the conduction state. The pulses had a unique width in the direction perpendicular to the director (the axis parallel to the average orientation) and had much larger and varying lengths parallel to the director.

Under nonequilibrium conditions, a spatially extended system often undergoes a transition from a uniform state to a state with spatial variation. We refer to this variation as a pattern. In nature, pattern formation is found in such diverse systems as cloud structures, snowflakes, flames, animal skins, and evolving populations. A fascinating aspect of patterns is that many of them have a universal character; physical, chemical, and biological systems all exhibit patterns that have many features in common. A deeper understanding of these features will help us to prevent undesirable patterns (or promote advantageous ones) in physical processes that affect our environment. From the viewpoint of fundamental science, patterns are of interest because their formation is generally associated with nonlinear effects, which lead to qualitatively new phenomena that do not occur in linear systems. Among the most fascinating of these phenomena is STC (1).

The elucidation of STC has been a main goal in nonlinear science since the mid-1970s, when it was first studied in fluid-mechanical systems (2). Loosely, we use the term STC to describe a deterministic system that has irregular variation and is unpredictable in detail, both in space and in time. Most known examples of STC occur as a result of a transition (or bifurcation) from a base state that already has an intricate but nonchaotic spatial variation. A theoretical analysis of STC is very difficult because it must begin at this already complicated starting point.

Here, we describe experimental observations of STC that (over a certain parameter range) evolves directly from the uniform state as the system is pushed beyond the first bifurcation. The STC consists of a superposition of four modes (see below)

that have spatially and temporally varying amplitudes with a mean square that grows continuously from 0 and whose time average is uniformly extended in space. In this case, it should be possible to elucidate the STC by weakly nonlinear theories that are applicable when amplitudes are small. These theories are well developed in the form of so-called complex Ginzburg-Landau (CGL) equations. Because the STC state evolves continuously from the uniform state, and because it consists of only a small number of modes, the relevant coupled CGL equations should be derivable from the full equations of motion (3) of the system (4). An example of the STC state at one instant of time is given in Fig. 1A.

We studied electroconvection (5) in the nematic liquid crystal (NLC) 4-ethyl-2-fluoro-4'-[2-(trans-4-pentylcyclohexyl)ethyl]-biphenyl (I52). The long, rodlike NLC molecules are orientationally ordered relative to their neighbors, but their centers of mass have no positional order. The axis parallel to the average orientation is called the director  $\hat{n}$ . We obtained a sample with uniform planar alignment of  $\hat{n}$  (parallel to the surfaces) by confining the NLC between two treated parallel glass plates. We used transparent conducting films on the inner surfaces of the glass plates and applied an ac voltage of amplitude  $V$  and frequency  $f$  between them. At a critical value  $V_c$ , a transition from a spatially uniform quiescent state to convection occurs. The precise value of  $V_c$  can be altered by changing  $f$  or by changing the electrical conductivity  $\sigma$ ; the conductivity can be changed either by adding small amounts of iodine to the I52 or by changing the temperature. Values of  $\sigma$  in our samples ranged from  $0.6 \times 10^{-8}$  to  $1.8 \times 10^{-8}$  ohm $^{-1}$  m $^{-1}$ .

Immediately above  $V_c$  and for  $\sigma \approx 1 \times 10^{-8}$  ohm $^{-1}$  m $^{-1}$ , we found oblique rolls with a wave vector  $\mathbf{k}$  at a nonzero angle  $\theta$  with respect to  $\hat{n}$  (6, 7). Because  $\hat{n}$  only gives an axis and does not specify a direc-

Department of Physics and Center for Nonlinear Science, University of California, Santa Barbara, CA 93106, USA.

\*To whom correspondence should be addressed.